Soft Matter

Soft Nanoconfinement of Ionic Liquids in Lyotropic Liquid Crystals

Journal:	*Soft Matter*
Manuscript ID	SM-ART-05-2021-000796.R2
Article Type:	Paper
Date Submitted by the Author:	31-Jul-2021
Complete List of Authors:	Bandegi, Alireza; New Mexico State University, Chemical and Materials Engineering; new mexico state university Marquez Garcia, Maria Guadalupe; New Mexico State University, Chemical and Materials Engineering Banuelos, Jose; University of Texas at El Paso, Physics Firestone, Millicent; Lawrence Berkeley Laboratory, ; Los Alamos National Laboratory, Materials Physics & Applications Foudazi, Reza; New Mexico State University, Chemical and Materials Engineering

Soft Nanoconfinement of Ionic Liquids in Lyotropic Liquid Crystals

Alireza Bandegi [a], Maria Marquez Garcia [a], Jose L. Bañuelos [b], Millicent A. Firestone [c,d], Reza Foudazi [a1]

[a] *Department of Chemical and Materials Engineering, New Mexico State University, Las Cruces, NM, 88003, United States*

[b] *Department of Physics, The University of Texas at El Paso, El Paso, TX, 79968, United States*

[c] *Lawrence Berkeley National Laboratory, Berkeley, CA, 94720, United States*

[d] *Materials Physics & Applications Division, Center for Integrated Nanotechnologies, Los Alamos National Laboratory, USA*

[1] Corresponding author. Email: rfoudazi@nmsu.edu.

Abstract

Nanoconfinement of ionic liquids (ILs) influences their physicochemical properties. In this study, we investigate the effect of soft nanoconfinement imposed by lyotropic liquid crystals (LLCs) on ILs. The LLC ion gels are obtained through self-assembly of a short chain block copolymer (BCP) of polyethylene-block-poly(ethylene oxide), PE-b-PEO, in ILs. The effect of confinement on the interaction of ions with PEO is investigated through electrochemical impedance spectroscopy (EIS) and carbon dioxide (CO_2) absorption measurements. The results show that the synergistic effect on the CO_2 absorption capacity of LLC ion gels takes place as a result of confinement. Formation of IL pathways through the LLC increases the CO_2 solubility, absorption capacity, and absorption rate. Increasing the concentration of block copolymer in LLC structure enhances the dissociation of ILs and consequently lower CO_2 absorption. Therefore, the competing effects of confinement and IL-PEO interaction control the properties of LLC ion gels.

Introduction

Ionic liquids (ILs) have been widely investigated as novel solvents, electrolytes, and soft functional materials due to their unique properties including high thermal stability, negligible vapor pressure, and high ionic conductivity.[1] However, the widespread applications of ILs have been hampered by their liquid state. A simple but versatile strategy to overcome this problem is to confine ILs in nanoporous host. Nanoconfinement of ILs can promote unusual charge transport and functionalities for IL-based devices for energy generation and storage.[1–4]

Comprehensive studies have been done on the behavior of ILs in pores of various sizes and types by molecular dynamic (MD) simulations.[1,5] The simulations have reported both a decrease[6,7] and an enhancement [8,9] in the ion mobilities of ILs confined in pores. Different experimental techniques have been used to understand the physicochemical properties and dynamics of nanoconfined ILs in various porous materials on a molecular level.[1] For example, using specialized nuclear magnetic resonance (NMR) techniques, Le Bideau et al. found a decrease in the diffusivity of ILs in monolithic silica matrices.[10] Iacob et al. showed an enhancement in the diffusion coefficients of ILs confined in silica nanopores by more than two orders of magnitude in comparison to their bulk values, which was attributed to the changes in ion packing under two-dimensional geometrical confinement.[11] These results show the importance of the pore sizes, pore wall-IL interaction, and physiochemical properties of ILs investigated under confinement.

In comparison to comprehensive studies on the structural dynamics of confined ILs in rigid inorganic matrices, the physicochemical aspects of soft nanoconfinement of ILs in polymer matrices have been overlooked. Polymer electrolytes are usually obtained by in situ polymerization of monomers in ILs [12–14] or solvent casting method.[15,16] Several polymers, such as poly(methyl methacrylate),[15,16] fluorinated copolymer poly-(vinylidene fluoride-co-chlorotrifluoroethylene),[16] and epoxy resins[13] have been explored. Among them, block copolymers (BCs) can form advanced assembled nanostructures driven by the affinity of a selective block to ILs, and thus, impose confinement on ILs.[17,18]

Several molecular dynamics simulation have been done on the structural and dynamics of polymer electrolytes based on PEO and ILs (homogeneous electrolytes in which IL is not confined).[19,20] It has been reported that upon formation of the polymer electrolytes, there is a remarkable slowdown of the polymer dynamics in comparison with pure PEO. This effect is attributed to the coordination of oxygen atoms of PEO chains with cations of ILs. Park et al. reported that breaking ionic clusters to achieve homogeneous ionic phase is a coherent method to enhance ion conductivity of polymer electrolytes.[21]

MD simulations have shown that gas diffusion in the confined gas/IL mixtures can be faster than that in the bulk.[8,9] Different experimental techniques have been used to understand the physicochemical properties and dynamics of nanoconfined ILs in various porous materials on a molecular level.[1,11,22–24] By using pulsed field gradient NMR, Hazelbaker and coworkers[22] found that, compared to the bulk condition, the diffusivities of CO_2 and IL decrease under nanoconfinement in KIT-6 silica that has pore size of 8.5 nm. This result was attributed to the reduced density of ionic liquid at the pore walls, which provides an additional free volume that can lead to fast CO_2 diffusion near the walls. In another study, Shin et al.[25] investigated the dynamics of the IL and CO_2 in the supported ionic liquid membranes, measured with two-dimensional infrared spectroscopy and Pump-Probe experiments. They observed that the structural fluctuations of the IL in the pores are slower than that in the bulk phase by ~ 2-fold. Their results showed that despite the relatively large pore size (~ 350 nm) of the membrane, the IL structural change induced by the polymer interface can propagate out from the interface more than 100 nm, influencing the dynamics of ILs.[25] In addition, macroscopic uptake and permeability measurements of CO_2 showed that the carbon dioxide transport in confined ILs can be faster than that in corresponding bulk ILs.[26,27] These observations suggest that confined ILs can perform better than bulk ILs for applications in gas capture and separations.

For a series of di-block copolymers comprising poly(styrensulfonate) (PSS) and poly(methylbutylene) (PMB), PSS-b-PMB, confinement effects could suppress the ion clustering

tendency if the PSS domain width was narrower than 6 nm.[21] The benefits of suppressing ion cluster formation to enhance proton transport properties were further demonstrated by employing phosphonated polymers.[28] Therefore, the break-up of ionic clusters with the aid of confinement is a promising approach to enhance the conductivity of polymer electrolyte.[29] The ILs confined in the gel polymer electrolyte can be divided into two fractions: (1) at (or close to) polymer /IL interface and (2) within IL domains. The interaction of the gel matrix with either cations or anions decreases the tendency to form ion-pairs or aggregates, resulting in an increase in the total number of ion carriers in the gel polymer electrolyte.[12,30,31]

It has been shown that CO_2 is remarkably soluble in imidazolium-based ILs.[32–35] For example, the solubility of CO_2 in 1-butyl-3-methylimidazolium hexafluorophosphate ([BMIM][PF_6]) at 15 bar pressure is about 23 mol%.[36] The CO_2 solubility can be tuned by variation of cations and anions. For example, using fluorine-containing anions (e.g., bis(trifluoromethylsulfonyl)imide, Tf_2N)[35] could increase the CO_2 solubility. In this work, therefore, we use 1-butyl-3-methylimidazolium hexafluorophosphate, [BMIM][PF_6], and 1-butyl-1- methylpyrrolidinium bis(trifluoromethylsulfonyl)imide, [BMPyr][NTF_2]. To make soft templates for nanoconfinement of ILs, we use Brij58, a di-block copolymer of PE and PEO. Due to the high polarity difference between the polar domains of the ILs and nonpolar n-alkyl tails of the di-block copolymer as well as hydrogen bonding of cations with ether oxygen of PEO, the phase segregation leading to self-assembled nanodomains is observed. Therefore, the obtained block copolymer and IL mixtures have lyotropic liquid crystal (LLC) state. We investigate the effect of soft nanoconfinement on the structural properties of ILs through electrochemical impedance spectroscopy (EIS) and CO_2 absorption measurements. We compare the IL nanoconfinement in LLCs with homogeneous mixtures of PEO/IL as control samples.

Experimental

Materials

Polyoxyethylene-20-cetyl ether known as Brij58 (M_n = 1124 g/mol, Sigma-Aldrich) was used as block copolymer. The polyethylene oxide (M_w=1000 g/mol, Sigma-Aldrich, PDI=1.07), which has approximately the same molecular weight of PEO block in Brij58, was used for the preparation of control samples. 1-Butyl-3-methylimidazolium hexafluorophosphate ([BMIM][PF_6], 98%, Sigma-Aldrich) and 1-butyl-1- methylpyrrolidinium bis(trifluoromethylsulfonyl)imide ([BMPyr][NTF_2], 98%, Sigma-Aldrich) were used as ILs. All chemicals were used as received without further purification. For preparation of samples, desired amounts of components were mixed manually until a homogeneous mixture was obtained. As control samples, homogeneous mixture of PEO/IL were prepared with the same ratio of PEO/IL (47/53) as in the Brij58/IL (52/48) samples.

X-ray Scattering

SAXS measurements were carried out using Bruker Nanostar System with a monochromated Cu Kα radiation source with the wavelength of 1.54184 Å. The q is the scattering vector defined as $q=4\pi\sin\theta/\lambda$, where θ is half the scattering angle. Samples were loaded into nominally 1.0 mm PTFE washers with Kapton windows. To prevent sample evaporation, vacuum isolation adapters were installed at the end of the primary flight path and entrance to the secondary flight path so that the samples were at ambient pressure within the ~10 cm air gap between the adapters during the SAXS measurements. In SAXS, X-rays scattered as function of the scattering angle 2θ, with respect to the transmitted direct beam, are collected on an area detector. The 2-D intensity data are azimuthally averaged and plotted as I(q). Corrections were applied to the sample data including normalization by transmission coefficient and count time, empty container and instrument background subtraction, thickness normalization, and scaling of the SAXS intensity, I(q), to units of differential scattering cross section per unit volume (cm^{-1}) using a glassy carbon intensity calibration standard.

Rheology

A stress-controlled rheometer DHR-3 (TA Instruments, New Castle, DE) was used to measure the rheology of samples. A 20 mm cross-hatched parallel plate geometry with 1 mm gap was used in all experiments. All tests are performed in the linear viscoelastic region (0.5% strain, confirmed from amplitude sweep tests). Frequency sweep tests were done on samples at 25 ºC and frequency range of 100 to 0.1 Hz.

Impedance Spectroscopy

The ionic conductivity was measured via EIS. The samples were placed into a Teflon ring, which held the samples at a constant diameter (6 mm) and thickness (2 mm). The sample disks were sandwiched between two stainless steel blocking electrodes. Sample temperature was maintained using a custom-built environmental chamber. The samples were held at each temperature for 1 h before measurement. The AC amplitude was 50 mV and the frequency were scanned from 1 MHz to 0.1 Hz.

Fourier transform IR (FTIR) spectroscopy

LLC Ion gels were studied by FT-IR ATR Perkin Elmer spectroscopy in the range 4000–600 cm^{-1}. Baseline correction was carried out on the IR spectra.

Absorption Measurement

The CO_2 uptake capacity of samples was measured with a Micromeritics ASAP2050 Xtended Pressure Instrument. We followed the procedure reported in the literature for measuring the CO_2 absorption of ILs.[37,38] Approximately 1 g of samples was used for measurement. Before analysis, the sample was degassed under vacuum at 70 ºC with pressure less than 10 μmHg. The degasification was stopped after the pressure increase rate was less than 1 μmHg/min. It takes approximately 24 h for complete degasification of samples. The absorption isotherms were obtained at room temperature (25 ºC) and gas pressures of up to 7500 mmHg. The temperature of the sample was controlled by circulating a mixture of ethylene glycol and diethylene glycol in

water to a Dewar flask in which the sample holder was drowned. The temperature of the flask was controlled by a thermostat with a precision of ± 0.01 C. The amount of CO_2 absorbed by the samples was calculated from the pressure change between the gas injection and equilibrium. The instrument performed dosing/vacuuming and equilibrium based on the target pressure. After initial pressure adjustment for each step, the instrument insolated the sample for equilibrium. The equilibration continued until the pressure variation in the sample holder was less than 0.1% per minute. The equilibrium check interval was assigned as 100 s. From the measured pressure change, the amount (moles) of gas absorbed was calculated via the ideal gas law. The amount of CO_2 desorbed by the samples was calculated from the pressure change during vacuum and equilibrium. The instrument performed vacuuming and equilibration based on the target pressure. The equilibration continued until the pressure variation in the sample holder was less than 0.1% per minute. The equilibrium check interval was assigned as 100 s.

Results and Discussion

SAXS Analysis

The selected ILs, [BMIM][PF_6] and [BMPyr][NTF_2], form lamellar structure with Brij58, in which the confinement size can be changed without losing the structure. Six different samples are investigated with different compositions. Table 1 summarizes the samples used in this study. The morphology of the LLC ion gels is lamellar structure as determined by SAXS (Figure 1a). Lamellar structures have 1:2:3… relative positions of Bragg peaks, q/q^*, where q^* is the principal peak. According to Bragg's equation, in lamellar structure, the lattice parameter, d, is calculated from $d=2\pi/q^*$ equation. The polar domain size, δ, can be estimated as $\delta = d\phi$, where ϕ is the volume fraction of polar domain (PEO block and IL). Detailed definition and calculations of parameters can be found elsewhere.[39–43] The calculated parameters obtained from SAXS experiments on various samples are summarized in Table 1.

The frequency sweep results show that $G' > G''$ for the samples, thus, the ion gels have a solid-like behavior in the linear viscoelastic region (Figure 1b and Figure S1). Block copolymers self-assemble in selective solvents and form mesophases. It has been reported that mixtures of Brij58 and water form LLC mesophases.[44] In this study, the ILs have been used as selective solvent for the formation of LLC structure. The cross-polarized light micrographs of ion gels confirm the formation of LLCs with mixture of Brij58 and ILs (Figure S2).

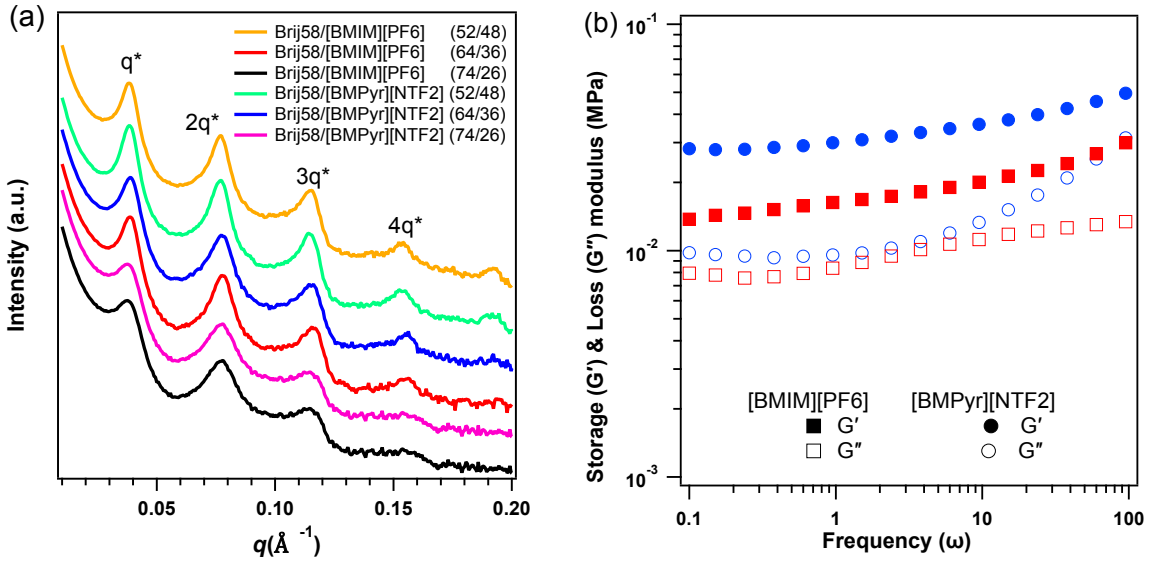

Figure 1. (a) SAXS profiles for the LLC ion gels at room temperature (25 °C). (b) The storage and loss moduli of ion gels prepared with Brij58/IL 74/26 wt%.

Table 1. SAXS characteristics of LLC ion gels.

Compositions (wt%)	Structure	d-spacing (nm)	Polar domain (nm)	D_{IL} (nm)
Brij 58/[BMPyr][NTF_2] (52/48)	Lamellar	16.2	12.6	6.5
Brij58/[BMPyr][NTF_2] (64/36)	Lamellar	16.4	13.4	4.8
Brij58/[BMPyr][NTF_2] (74/26)	Lamellar	15.8	12.1	3.2
Brij58/[BMIM][PF_6] (52/48)	Lamellar	16.4	12.8	6.5
Brij58/[BMIM][PF_6] (64/36)	Lamellar	16.3	13.4	4.7
Brij58/[BMIM][PF_6] (74/26)	Lamellar	15.8	13.0	3.2

Confinement in LLC ion gels

To investigate the effect of soft nanoconfinement in our system, the IL pathway thickness (D_{IL}) and chain density are calculated (Table 1). The D_{IL} is the intermicellar distance and is obtained from $D_{IL} = \varphi_{IL} d$ (Figure 2).

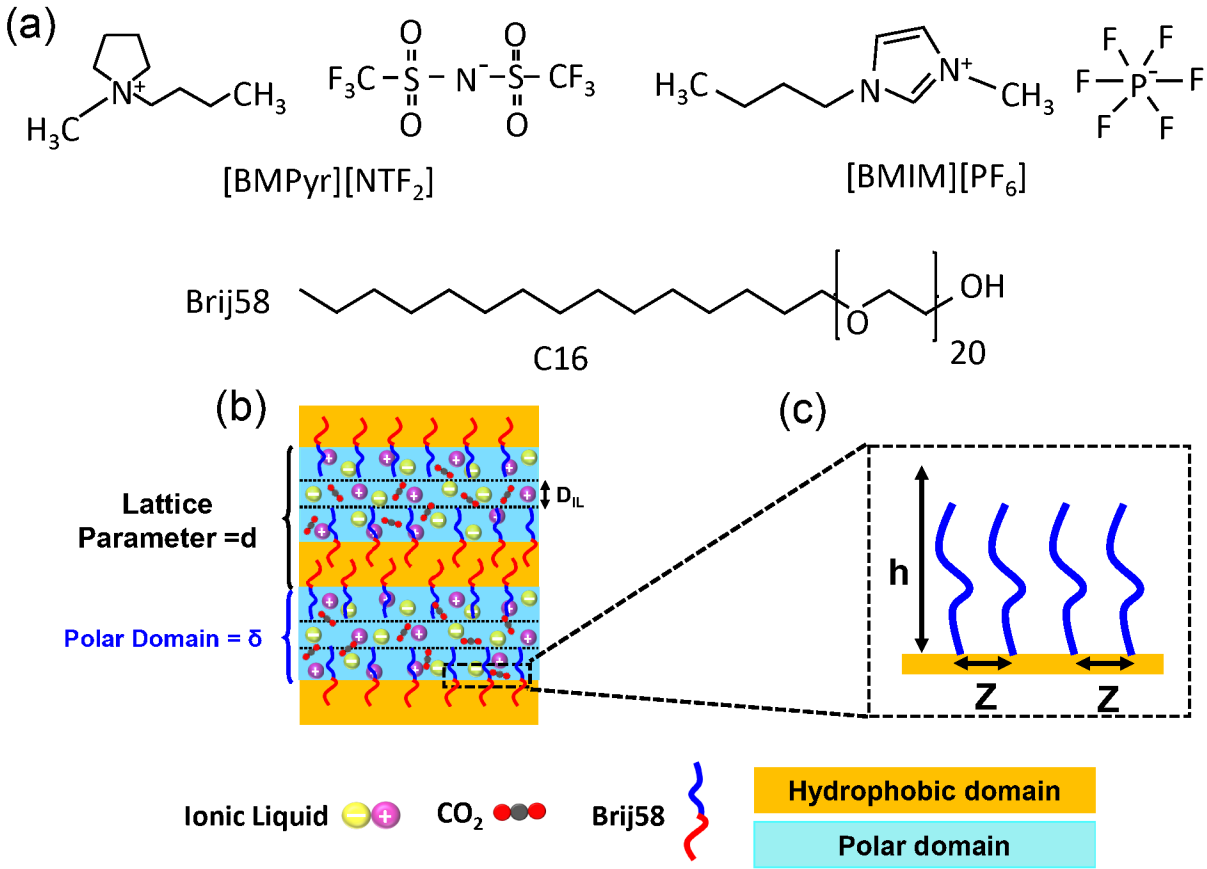

Figure 2. (a)The chemical structure of ILs and Brij58, (b) schematic representation of the lamellar structure in LLC ion gels, and (c) planar chain density of PEO in polar domain.

We hypothesize that densely tethered chains stretch to alleviate the interactions caused by crowding.[45] A random coil conformation (mushroom regime) occurs when the interchain distance (Z) is greater than $2R_F$ (where R_F is the Flory radius), and more extended conformation (brush regime) occurs when $Z < 2R_F$.[46] The stretching-entropy and excluded-volume interactions

influence the chain density in the brush regime as result of lateral confinement. The Flory radius (R_F) can be estimated using following equation:[46]

$$R_F = b\,N^{\upsilon} \quad (1)$$

where b is the characteristic monomer dimension (taken as 2.78 Å for the ethylene oxide repeating unit), N is the number of monomers in each PEO chain, and υ is taken as 0.5. The Flory radius for the PEO chains pendant in polar domain with molecular weight of 1000 g/mole is estimated to be 1.3 nm. The interchain distance inversely scales with chain density. The distance between the grafting sites, Z, can be obtained as follows:[47]

$$Z = \frac{2}{\sqrt{\pi\sigma}} \quad (2)$$

where σ is the planar chain density (with unit of nm^{-2}), which can be obtained from mass balance equation given as follows:[47]

$$\sigma = \frac{\rho h N_a}{M_n} \quad (3)$$

where $h = \frac{\delta - D_{IL}}{2}$ is the thickness of polymer brush, ρ is the bulk density of polymer, N_a is Avogadro number, and M_n is the number average molecular weight of polymer brush.

Table 2. The density and physical distance of PEO chains in polar domains of LLC ion gels with different compositions.

Compositions (wt%)	h (brush thickness, nm)	σ (chain density, nm^{-2})	Z (interchain distance, nm)
Brij 58/[BMPyr][NTF_2] (52/48)	3.1	2.3	0.7
Brij58/[BMPyr][NTF_2] (64/36)	4.3	3.2	0.6
Brij58/[BMPyr][NTF_2] (74/26)	4.5	3.4	0.6
Brij 58/[BMIM][PF_6] (52/48)	4.6	3.5	0.6
Brij 58/[BMIM][PF_6] (64/36)	4.8	3.6	0.6
Brij 58/[BMIM][PF_6] (74/26)	4.9	3.7	0.6

From Eq. (2) and (3), we can estimate the interchain distance of PEO in the polar domains of the LLC ion gels with different composition (Table 2). The interchain distance of the PEO chains for

all the LLC ion gels are lower than the Flory radius ($Z < 2R_F$), implying that PEO chains in all samples are in brush regime and the chains have extended conformation. By increasing the block copolymer concentration, the D_{IL} in the polar domain becomes smaller.

Nanostructure Effect

The confinement of ILs, where ion-wall interactions become important relative to ion-ion interactions, can induce some changes in their physicochemical behavior.[48–50] It has been reported that the addition of IL to pure PEO slows down polymer dynamics.[51] This retardation in polymer dynamics was attributed to the coordination between the cations and the polymer backbone. Such a strong coordination can be expected to hinder the mobility of the polymer backbone and reflect in slower polymer relaxation.[51] To investigate the effect of soft nanoconfinement on the interactions between the ions and PEO chains in LLC ion gels, the relaxation time of the polymer chains is measured through EIS. Dielectric relaxation is a result of the reorientation process of dipoles in the polymer chains, which shows a shoulder in ε'' spectra (Figure 3a).[52] By increasing the temperature, the peak in ε'' spectra shifts to higher frequency suggesting the acceleration of the relaxation process (Figure S3).[52] The complex permittivity spectra of the ion gels are analyzed utilizing the empirical Havriliak-Negami (HN) function.

$$\varepsilon^*(\omega) = \varepsilon_\infty + \frac{\Delta\varepsilon}{\left[1 + (i\omega\tau_{HN})^\alpha\right]^\beta} \quad (4)$$

where τ_{HN} is the characteristic relaxation time, $\Delta\varepsilon = \varepsilon_0 - \varepsilon_\infty$ is the relaxation strength of the process in which $\varepsilon_0 = \lim_{\omega\to 0} \varepsilon'(\omega)$ and $\varepsilon_\infty = \lim_{\omega\to\infty} \varepsilon'(\omega)$., and α and β $(0 < \alpha,\ \alpha\beta \leq 1)$ describe the symmetric and asymmetric broadening of the distribution, respectively.

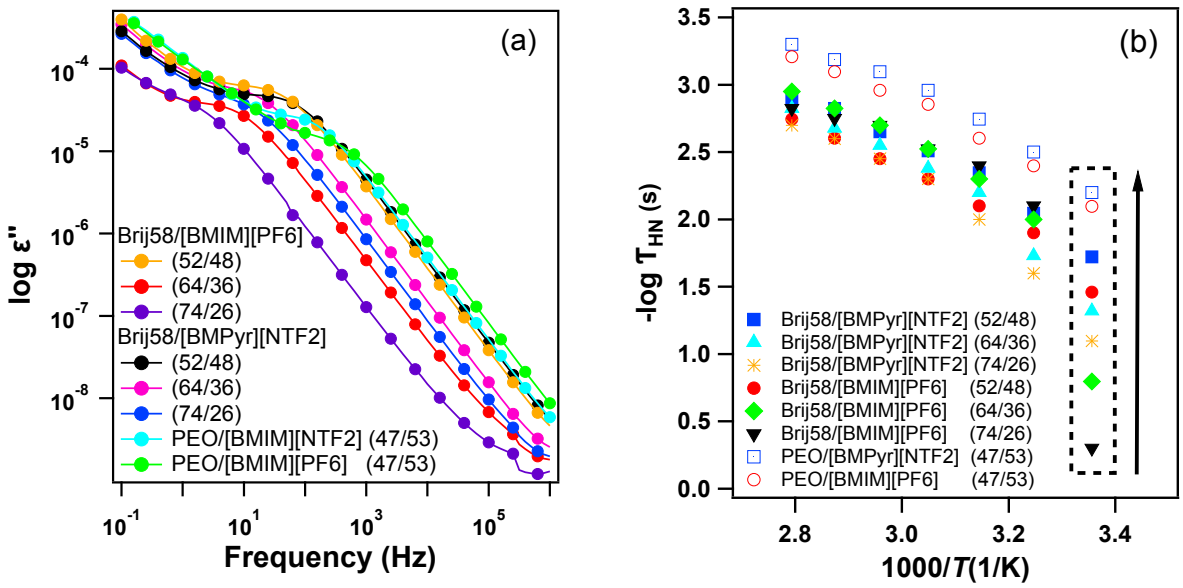

Figure 3. (a) The dielectric loss spectra $\varepsilon''(\omega)$ of ion gels versus frequency at room temperature, (b) The temperature dependence of relaxation time for LLC ion gels and PEO/IL mixture. The arrow shows the direction from slow to fast relaxation time.

The relaxation strength of the process is determined from the step in the real permittivity data. Then, the relaxation time is obtained by fitting the imaginary part of the Havriliak-Negami equation with the imaginary permittivity data.[53] With increasing the temperature, the dielectric strength of the electrolyte increases while the relaxation time becomes faster (Figure 3b), which confirms the enhancement of ionic polarization.[54] Mostly in polymer electrolytes, the ionic conduction occurs in the presence of local segmental motions of the polymer host, which is due to a direct coupling between ions and functional group of the polymer.[55] PEO exhibits a Vogel-Fulcher-Tamman (VFT) relaxation (i.e., α relaxation) process attributed to large-scale cooperative segmental motion of PEO chains above its melting point.

Figure 3b shows that the relaxation time of PEO chains is slower in LLC ion gels compared to the homogeneous mixtures of PEO/IL. The configuration of PEO chains in the nanodomains of LLC ion gels is strongly affected by the thermodynamic interactions.[56] Therefore, the motion of PEO chains in LLC ion gels inevitably coupled with the surrounding chains to minimize the density

fluctuations. This phenomenon possibly leads to retarded relaxation of PEO chains in LLC ion gels compared to homogeneous mixture of PEO/IL.[56] One important observation from Figure 3b is that the PEO relaxation time in LLC ion gels prepared with [BMIM][PF_6] is slower than that of [BMPyr][NTF_2] at each composition. The difference in relaxation times is attributed to the stronger hydrogen bonding of [BMIM][PF_6] with alkyl hydrogen of PEO chains compared to the [BMPyr][NTF_2], restricting the segmental motion of the polymer chains.[57]

The FTIR analysis have been done to further investigate the interaction of ILs with PEO chains in the LLC ion gels. The FTIR results (Figure 4) show that a hydrogen bonding forms between the alkyl hydrogen of PEO and the fluorine ions of $[PF_6]^-$ and $[NTF_2]^-$. The hydrogen bonding is also possible between cations (especially imidazolium-based ones) and PEO chains.[58] Therefore, one expects that a stronger hydrogen bonding is detected when the Brij58 concentration is increased in the ion gels. The results show that by increasing the Brij58 concentration in the Brij58/[BMIM][PF_6] ion gels, the intensity of C-H stretching peak significantly decreases and the peaks become broader, which confirms the enhancement of interaction of $[PF_6]^-$ and/or $[BMIM]^+$ with the PEO chains. The change in C-H stretching peak is not significant for $[NTF_2]^-$ anions in the studied range of Brij concentration, which suggests that [BMPyr][NTF_2]-PEO interaction is weaker than [BMIM][PF_6]-PEO one.

To further investigate the effect of soft nanoconfinement on the interaction of ions with PEO, the number of free ions in the system have been estimated from EIS data. The frequency dependent dielectric spectra are analyzed with Random Barrier Model proposed by Dyre[59] to extract the dc conductivity σ_0 and ion diffusion rate $1/\tau_e$., where τ_e is the relaxation time.

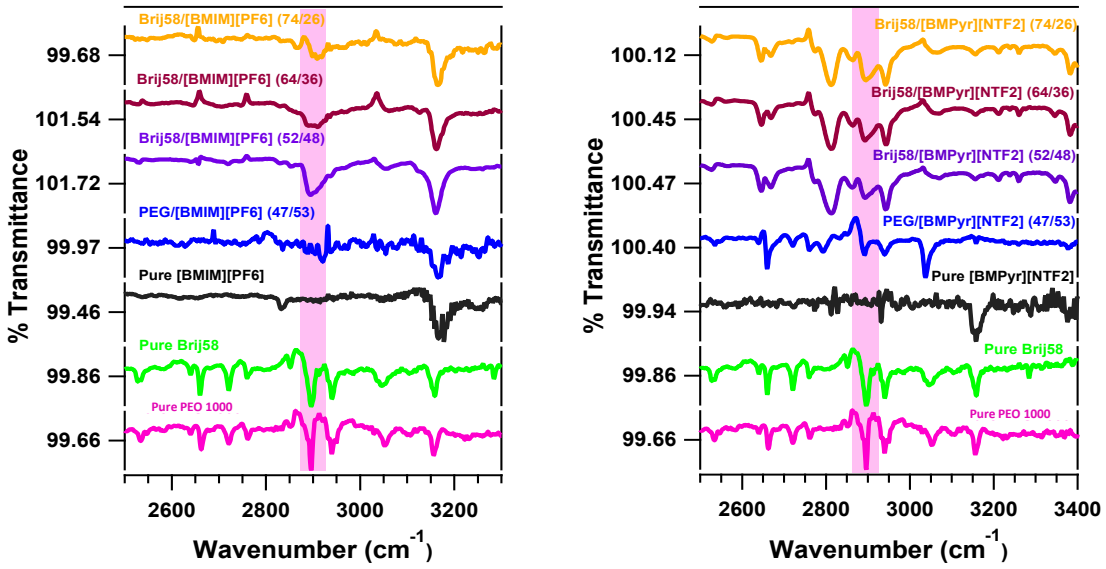

Figure 4. FTIR spectra of ion gels with different compositions and ionic liquids. The shaded area is from the spectral regions of C-H stretching. The spectrums are vertically shifted for comparison.

The Random Barrier Model assumes that the conduction takes place by hopping of charge carriers in a spatially randomly varying energy landscape and provides an approach to analyze the conduction on a theoretical level. Within the Continuous-Time-Random Walk (CTRW) approximation,[60] the following expression for the complex conductivity is obtained[59]:

$$\sigma^*(\omega) = \sigma_0\left[\frac{i\omega\tau_e}{\ln(1+i\omega\tau_e)}\right] \quad (5)$$

Splitting into real and imaginary parts delivers:

$$\sigma'(\omega) = \frac{\sigma_0\omega\tau_e \arctan(\omega\tau_e)}{\frac{1}{4}\ln^2(1+\omega^2{\tau_e}^2) + (\arctan(\omega\tau_e))^2} \quad (6)$$

$$\sigma''(\omega) = \frac{\sigma_0\omega\tau_e \ln(1+\omega^2{\tau_e}^2)}{\frac{1}{2}\ln^2(1+\omega^2{\tau_e}^2) + 2(\arctan(\omega\tau_e))^2} \quad (7)$$

Equations (6) and (7) are used to fit the data present in Figure 5 and Figure S4 and S5, to obtain σ_0 and τ_e (Table S1). Substantial deviation from Eq. (6) occurs at low frequencies. To describe

the spectra in the whole frequency region, more sophisticated models[61] should be considered. However, it should be emphasized that the main goal here is to evaluate free-ion number density from EIS data, which can be essentially captured by the Eq. (6) as shown in Figure 5. Here, the low-frequency response does not affect the analysis results.

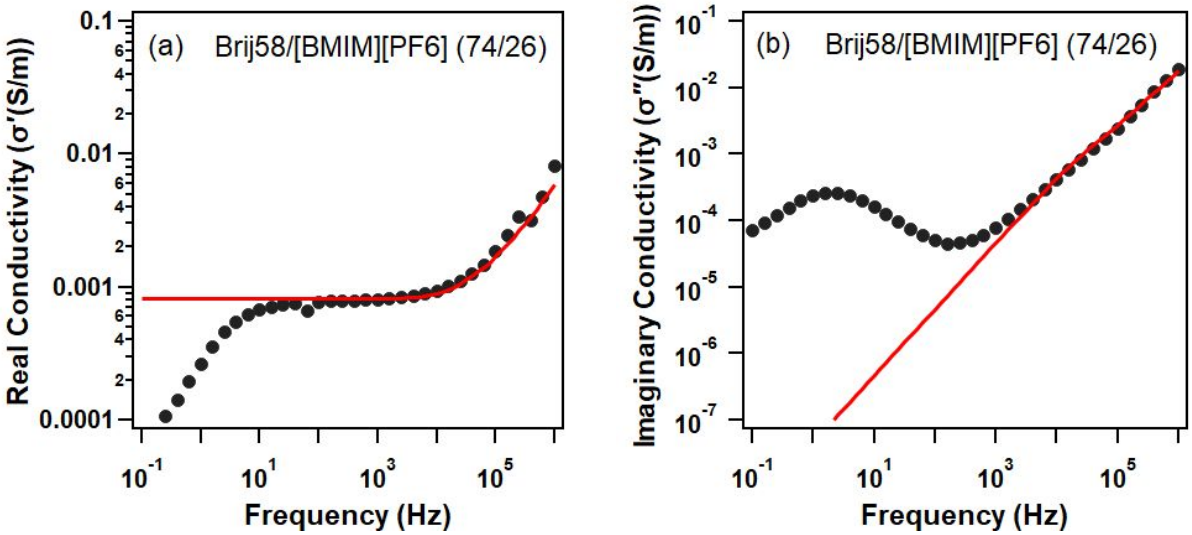

Figure 5. Typical (a) real and (b) imaginary parts of the complex conductivity spectrum, σ(ω). The solid red line is the fit to the spectrum using eq (6) and (7).*

It has been suggested that the free ion concentration and ionic diffusivity can be quantitatively determined by using relaxation time τ_e and dc conductivity σ_0.[62] In this method, to calculate the free ion concentration, we combine the electrodynamic analog of the Einstein relation:

$$\sigma_0 = \left(1/k_B T\right)\left(n_+ D_+ q_+^2 + n_- D_- q_-^2\right) \quad (8)$$

with the Einstein-Smoluchowski relation:

$$D = \lambda^2/2\tau_h \quad (9)$$

where k_B is the Boltzmann constant, $n_{+,-}$ is the free ion concentration, $q_{+,-}$ is the ion charge, $D_{+,-}$ is the ion diffusivity, λ is the ion jump length, and $1/\tau_h \approx 1/\tau_e$ is the mean ion hopping rate. Assuming that $D_+ \approx D_- = D$ (which has been demonstrated experimentally for many ILs),[63] n_+

$= n_- = n$, and $q_+ = q_- = e$ (the elementary charge), we arrive at the following expression connecting the free ion concentration, dc conductivity, and ion hopping rate:

$$\sigma_0 = \frac{2ne^2D}{k_BT} = \frac{ne^2\lambda^2}{k_BT\tau_e} \quad (10)$$

The total free ion concentration ($n_{total} = n_+ + n_-$) is calculated by taking the hopping length values, λ, comparable to the Pauling diameter. The results for λ reported by Sangoro et al.[64] for ILs varied between 0.24 and 0.31 nm. However, it has been reported that the hopping length is higher in polymeric electrolytes compared to pure ILs.[65] Based on the reported values in the literature for polymer electrolytes,[65–68] here we consider λ between 0.7 to 0.9 nm for our LLC ion gels. We consider this range to approximate and compare the fraction of free ions in our system with two different ILs. The 0.9 nm upper limit is the highest value reported for jump length in the literature for polymer electrolyte. The 0.7 nm lower limit for λ is chosen based on the fact that the number density of free ions obtained in this range from Dyre model would not be higher than the total number of ions in the system, which is determined from the density and the molecular weight of ILs at room temperature as follows:

$$n_{total-[BMIM][PF6]} = 2 \times \frac{\rho(g/m^3)}{MW(g/mol)} \times N_A = 2 \times \frac{1.38 \times 10^6}{284} \times 6.022 \times 10^{23} = 5.8 \times 10^{27}\ (Number\ of\ ions/m^3)$$

$$n_{total-[BMPyr][NTF2]} = 2 \times \frac{\rho(g/m^3)}{MW(g/mol)} \times N_A = 2 \times \frac{1.4 \times 10^6}{422} \times 6.022 \times 10^{23} = 3.9 \times 10^{27}\ (Number\ of\ ions/m^3)$$

Figure 6 and Table S2 show the results for the amounts of free ions in ion gels and PEO/ILs mixtures which are obtained from Eq (10). The same trend from the relaxation time can be observed for the number of free ions in the samples. The samples with slower relaxation time (e.g., Brij58/[BMIM][PF_6], 74/26 wt%) have higher free ions concentration due to the higher interaction of the ions with PEO, which enhances the dissociation of ion pairs. In other words, the samples with faster relaxation time (e.g., Brij58/[BMIM][PF_6], 52/48 wt%) have lower free ion

concentration. In addition, with increasing the Brij58 concentration, there is more enhancement in the number of free ions in Brij58/[BMIM][PF_6] ion gels compared to Brij58/[BMPyr][NTF_2]. This result is in agreement with the FTIR results in which increasing the Brij58 concentration in Brij58/[BMIM][PF_6] ion gels results in reduction of C-H stretching intensity. Therefore, it can be concluded that the interaction between the /[BMIM][PF_6] and PEO chains is stronger compared to [BMPyr][NTF_2] and PEO. Consequently, by increasing the Brij58 concentration, a higher portion of [BMIM][PF_6] is dissociated in the ion gel compared to [BMPyr][NTF_2].

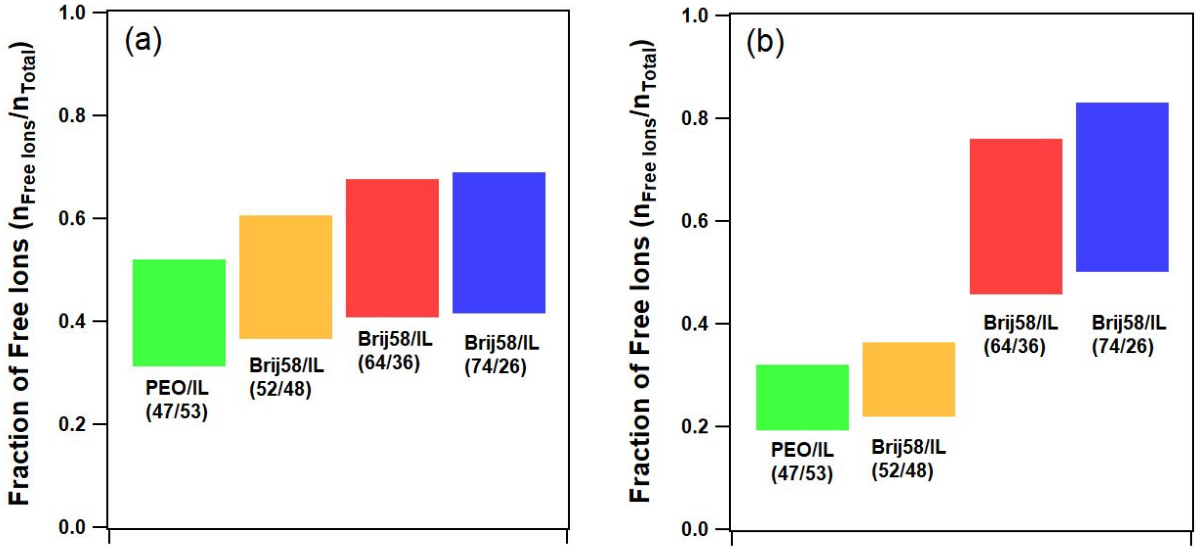

Figure 6. The fraction of free ions obtained from Dyre Model with the λ in the rage of 0.7 to 0.9 nm for LLC ion gels and PEO/IL mixtures prepared with (a) [BMPyr][NTF2] and (b) [BMIM][PF6].

Absorption Measurement

To further explore the effect of soft nanoconfinement on the structural properties of ILs, the CO_2 absorption capacity of ion gels are measured. The absorption-desorption data are presented in Figure S6. Figure 7 and Table S3 show the absorption data of CO_2 in LLC ion gels and PEO/IL mixtures at 25 ºC. The CO_2 absorption in LLC ion gels and PEO/IL mixtures is higher than that of the pure ILs even for the [NTF_2] anion with two CO_2-philic fluoroalkyl groups.[69] The enhanced absorption in LLC ion gels compared to PEO/ILs mixtures can be explained by the formation of

IL pathways between the polymer chains. Using the mixing rule, the amount of enhanced absorption compared to the pure components of the mixtures (i.e., PEO, Brij58, and IL) is calculated as follows:

$$\Delta\delta = x_{exp.} - \sum_{i=1}^{2} m_i x_i \quad (11)$$

where $\Delta\delta$ is the enhanced CO_2 uptake due to the synergistic effect, m_i is the weight percent of pure components in the mixtures, and x_i is the measured total CO_2 uptake of pure components. The $x_{exp.}$ is the total absorption obtained from the experiment and the $\sum_{i=1}^{2} m_i x_i$ is the absorption calculated based on mixing rule. The positive value of $\Delta\delta$ demonstrates that there is a synergistic effect on enhancement of the CO_2 uptake. As see in Figure 7, even with the same concentration of IL and EO groups in the mixtures, the normalized (with pressure) absorption of CO_2 in LLC ion gels is higher compared to the PEO/IL mixtures (Figure S7 shows the unnormalized absorption at 10 bar pressure). In addition, LLC ion gels show higher synergistic effect in absorption than the PEO/IL mixture. The enhancements in total amount of absorption and synergist effect in LLC ion gels are attributed to the formation of IL pathway between the PEO chains (Figure 2).

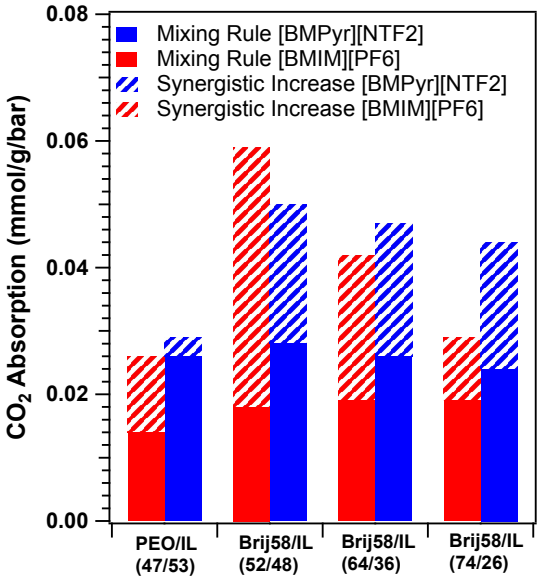

Figure 7. Total normalized CO_2 absorption of LLC ion gels. The contributions from mixing rule and synergistic effect in total absorption are shown by solid fill and diagonal stripes, respectively.

Molecular dynamic simulations have shown that the CO_2 solubility in ILs is not governed by a direct interaction between CO_2 and the ion;[70] rather, it is related to the unoccupied space (or free volume) in the IL phase.[36,71] A slight ion displacement in the IL phase expands the free volume throughout the IL domain. Therefore, more CO_2 molecules can be dissolved in the IL phase.

Comparing the trend in the number density of free ions in Figure 6 with the trend in the absorption results from Figure 7 reveals some information about the effect of soft nanoconfinement on structural properties of ILs. Increasing the Brij58 concentration in LLC ion gels prepared with [BMIM][PF_6] enhances the ions dissociation in the system (i.e., the free ion concentration increases). The results suggest that the dissociation of ILs in the ion gels deteriorate the CO_2 dissolution. For example, in sample Brij58/[BMIM][PF_6] with 74/26 wt% ratio, there is higher number of free ions compared to Brij58/[BMIM][PF_6] with 52/48 wt% ratio. The former contains higher IL dissociation, which results in lower absorption of CO_2.

As seen in Figure 6, there is not a significant difference between the free ion concentrations of LLC ion gels prepared with [BMPyr][NTF_2] at different compositions. This observation is in agreement with FTIR results in which the intensity of C-H stretching peak has not changed by increasing the Brij58 concentration in these ion gels. These results are also in agreement with the CO_2 absorption results in which the synergistic effect has not changed significantly by increasing the Brij58 concentration in the Brij58/[BMPyr][NTF_2] system.

The total elapsed time of the absorption measurements is investigated to understand how the rate of CO_2 uptake is different between the LLC ion gels and PEO/IL mixtures. The results show that the ion gels of Brij58/[BMIM][PF_6] and Brij58/[BMPyr][NTF_2] with 52/48 (wt:wt) compositions

412 have the highest absorption rate of 3.2 and 3.8 μmol/minute (Figure 8 and Table S4), respectively.

413 The desorption rates of these ion gels are also the highest compared to the other ion gels.

414

415

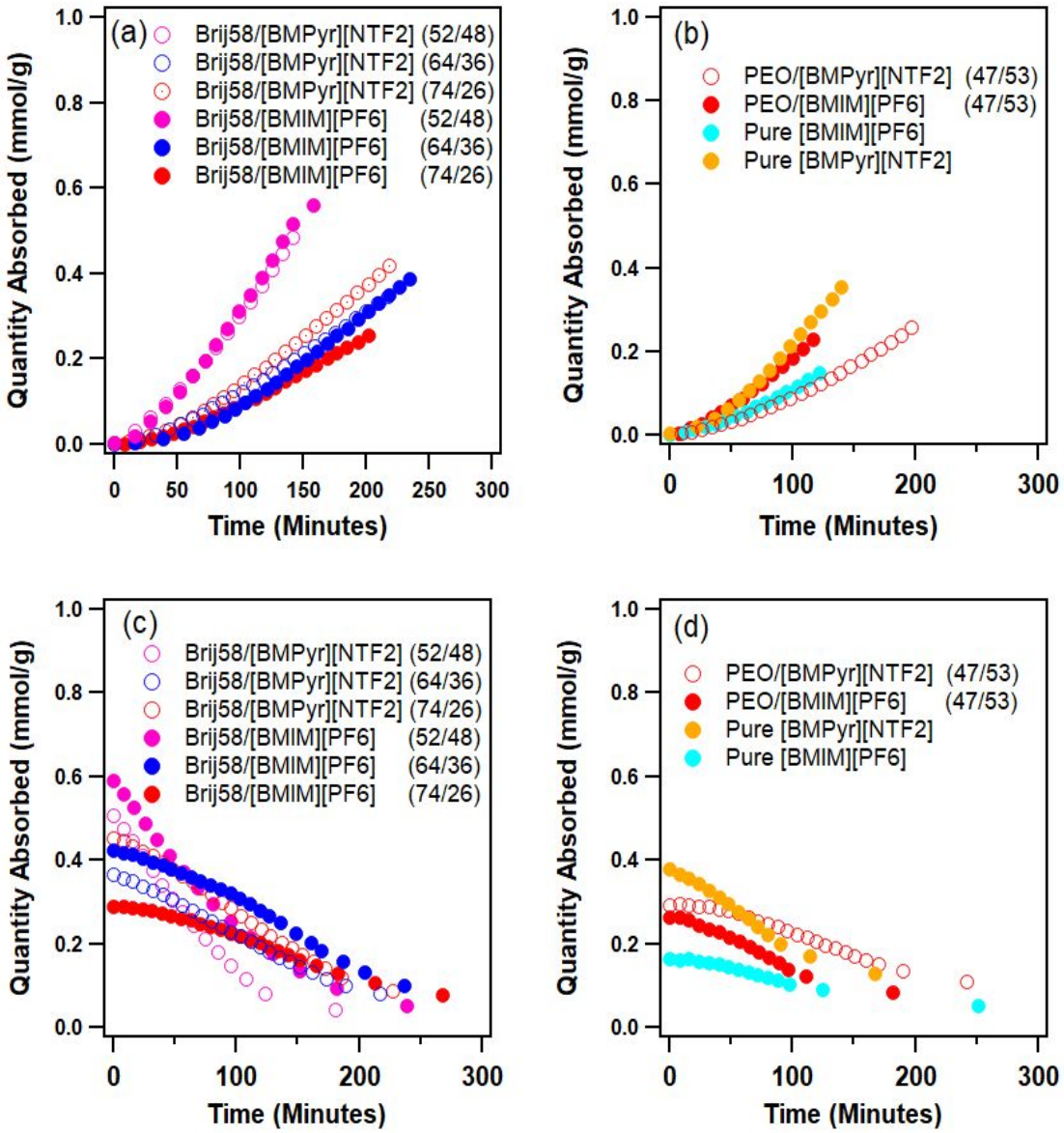

416

417

418 *Figure 8. Total elapsed time for (a,b) absorption of CO_2 in LLC ion gels and PEO/IL mixtures*

419 *and (c,d) desorption of CO_2 from LLC ion gels and PEO/IL mixtures.*

To investigate the relation between the viscosity and absorption-desorption rate of ion gels, the viscoelastic properties of samples have been measured through frequency sweep test (Figure S8). The rheological results (Table S4) prove that the viscosity is not the only factor affecting the absorption-desorption rate. For example, while the PEO/ILs mixtures have very low viscosity compared to ion gels, their absorption-desorption rate is lower than some of the ion gels (Figure 9).

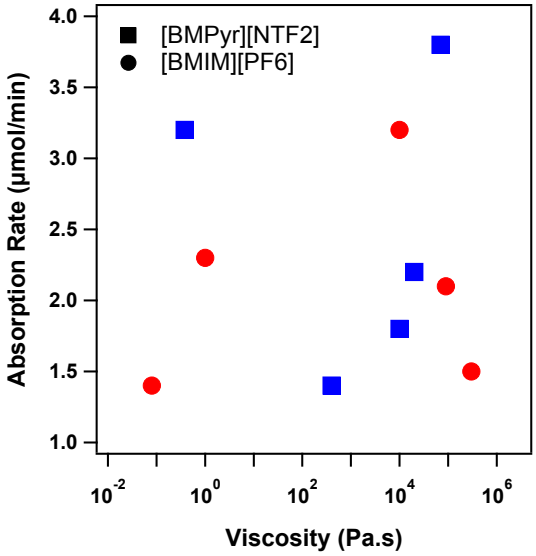

Figure 9. Absorption rate versus viscosity at frequency of 0.1 Hz for ion gels prepared with [BMIM][PF_6] and [BMPyr][NTF_2].

The same phenomenon can be observed for pure ILs. The [BMPyr][NTF_2] has higher absorption-desorption rate compared to [BMIM][PF_6] even though the former has higher viscosity. This is because of the higher solubility of CO_2 in [BMPyr][NTF_2] compared to [BMIM][PF_6]. These results confirm our discussion about the effect of soft nanoconfinement on the CO_2 uptake capacity of ion gels. Formation of IL pathways between the PEO chains through the LLC templating improves the solubility of CO_2 in ion gels and increases the absorption capacity and rate. However, there is an optimum for the concentration of block copolymer in the ion gels due to the dissociation of ILs, which deteriorates the CO_2 dissolution and consequently reduces the CO_2 capture capacity. The

prepared ion gel materials can be used in future as a platform for making gas separation membranes.[72–74]

Conclusion

We showed that the nanostructured ion gels have higher CO_2 absorption capacity compared to the pure ILs and homogeneous PEO/IL mixtures due to the existence of IL pathways between the PEO chains. In the studied systems, the criteria for obtaining an enhanced CO_2 absorption is to form confined domains of IL, which requires formation of LLCs. To form an LLC from block copolymer surfactant and IL mixtures, the IL needs to be a selective solvent for one of the blocks. In this work, the IL was a selective solvent for PEO block. Depending on the concentration of mixtures, different mesophases form which can induce confinement of IL in nano-size domains. The studied mesophase in this work was limited to lamellar structure with relatively wide range of IL domain size (i.e., confinement size). We found that the soft nanoconfinement effect appears to change the physical properties of the ILs through reorganization of the cations and anions at the interface. Increasing the block copolymer concentration in LLC ion gels leads to the dissociation of ILs, decreasing total absorption capacity and synergistic effect. Two competing effects of confinement and IL-PEO interaction control the properties of LLC ion gels. While the former enhances the CO_2 uptake, the latter lowers it. Owing to the nonvolatility, thermal stability, and tunable chemistry of block copolymers, LLCs from BCP/IL are very attractive candidates to design a platform for confinement of ILs for gas separation membranes.

Acknowledgement

Our work was supported through a grant by New Mexico NASA EPSCoR Research Infrastructure Development (RID), Cooperative Agreement Number 80NSSC19M0181. This work was performed in part at the Center for Integrated Nanotechnologies (CINT). CINT is funded by the DOE Office of Basic Energy Sciences LANL is operated by Los Alamos National Security, LLC,

for the National Nuclear Security Administration of the U.S. Department of Energy under contract DE-AC52-06NA25396.

Conflict of interest

The authors declare that they have no conflicts of interest.

References

(1) Zhang, S.; Zhang, J.; Zhang, Y.; Deng, Y. Nanoconfined Ionic Liquids. *Chem. Rev.* **2017**, *117* (10), 6755–6833.

(2) Gao, N.; He, Y.; Tao, X.; Xu, X.-Q.; Wu, X.; Wang, Y. Crystal-Confined Freestanding Ionic Liquids for Reconfigurable and Repairable Electronics. *Nat. Commun.* **2019**, *10* (1), 547.

(3) Futamura, R.; Iiyama, T.; Takasaki, Y.; Gogotsi, Y.; Biggs, M. J.; Salanne, M.; Ségalini, J.; Simon, P.; Kaneko, K. Partial Breaking of the Coulombic Ordering of Ionic Liquids Confined in Carbon Nanopores. *Nat. Mater.* **2017**, *16* (12), 1225–1232.

(4) MacFarlane, D. R.; Forsyth, M.; Howlett, P. C.; Kar, M.; Passerini, S.; Pringle, J. M.; Ohno, H.; Watanabe, M.; Yan, F.; Zheng, W.; et al. Ionic Liquids and Their Solid-State Analogues as Materials for Energy Generation and Storage. *Nat. Rev. Mater.* **2016**, *1* (2), 15005.

(5) Otero-Mato, J. M.; Montes-Campos, H.; Cabeza, O.; Gallego, L. J.; Varela, L. M. Nanoconfined Ionic Liquids: A Computational Study. *J. Mol. Liq.* **2020**, *320*,

114446.

(6) Rodriguez, J.; Elola, M. D.; Laria, D. Ionic Liquid Aqueous Solutions under Nanoconfinement. *J. Phys. Chem. C* **2012**, *116* (9), 5394–5400.

(7) Li, S.; Han, K. S.; Feng, G.; Hagaman, E. W.; Vlcek, L.; Cummings, P. T. Dynamic and Structural Properties of Room-Temperature Ionic Liquids near Silica and Carbon Surfaces. *Langmuir* **2013**, *29* (31), 9744–9749.

(8) Shi, W.; Luebke, D. R. Enhanced Gas Absorption in the Ionic Liquid 1-n-Hexyl-3-Methylimidazolium Bis(Trifluoromethylsulfonyl)Amide ([Hmim][Tf2N]) Confined in Silica Slit Pores: A Molecular Simulation Study. *Langmuir* **2013**, *29* (18), 5563–5572.

(9) Shi, W.; Sorescu, D. C. Molecular Simulations of CO2 and H2 Sorption into Ionic Liquid 1-n-Hexyl-3-Methylimidazolium Bis(Trifluoromethylsulfonyl)Amide ([Hmim][Tf2N]) Confined in Carbon Nanotubes. *J. Phys. Chem. B* **2010**, *114* (46), 15029–15041.

(10) Le Bideau, J.; Gaveau, P.; Bellayer, S.; Néouze, M.-A.; Vioux, A. Effect of Confinement on Ionic Liquids Dynamics in Monolithic Silica Ionogels: 1H NMR Study. *Phys. Chem. Chem. Phys.* **2007**, *9* (40), 5419–5422.

(11) Iacob, C.; Sangoro, J. R.; Kipnusu, W. K.; Valiullin, R.; Kärger, J.; Kremer, F. Enhanced Charge Transport in Nano-Confined Ionic Liquids. *Soft Matter* **2012**, *8* (2), 289–293.

(12) Susan, M. A. B. H.; Kaneko, T.; Noda, A.; Watanabe, M. Ion Gels Prepared by in Situ Radical Polymerization of Vinyl Monomers in an Ionic Liquid and Their Characterization as Polymer Electrolytes. *J. Am. Chem. Soc.* **2005**, *127* (13), 4976–4983.

(13) Matsumoto, K.; Endo, T. Confinement of Ionic Liquid by Networked Polymers Based on Multifunctional Epoxy Resins. *Macromolecules* **2008**, *41* (19), 6981–6986.

(14) Guyomard-Lack, A.; Buchtová, N.; Humbert, B.; Le Bideau, J. Ion Segregation in

an Ionic Liquid Confined within Chitosan Based Chemical Ionogels. *Phys. Chem. Chem. Phys.* **2015**, *17* (37), 23947–23951.

(15) Wang, X.; Akhmedov, N. G.; Duan, Y.; Luebke, D.; Li, B. Immobilization of Amino Acid Ionic Liquids into Nanoporous Microspheres as Robust Sorbents for CO2 Capture. *J. Mater. Chem. A* **2013**, *1* (9), 2978–2982.

(16) Yang, J.; Pruvost, S.; Livi, S.; Duchet-Rumeau, J. Understanding of Versatile and Tunable Nanostructuration of Ionic Liquids on Fluorinated Copolymer. *Macromolecules* **2015**, *48* (13), 4581–4590.

(17) Zhang, S.; Lee, K. H.; Sun, J.; Frisbie, C. D.; Lodge, T. P. Viscoelastic Properties, Ionic Conductivity, and Materials Design Considerations for Poly(Styrene-b-Ethylene Oxide-b-Styrene)-Based Ion Gel Electrolytes. *Macromolecules* **2011**, *44* (22), 8981–8989.

(18) Zhang, S.; Lee, K. H.; Frisbie, C. D.; Lodge, T. P. Ionic Conductivity, Capacitance, and Viscoelastic Properties of Block Copolymer-Based Ion Gels. *Macromolecules* **2011**, *44* (4), 940–949.

(19) Costa, L. T.; Ribeiro, M. C. C. Molecular Dynamics Simulation of Polymer Electrolytes Based on Poly(Ethylene Oxide) and Ionic Liquids. I. Structural Properties. *J. Chem. Phys.* **2006**, *124* (18), 184902.

(20) Costa, L. T.; Ribeiro, M. C. C. Molecular Dynamics Simulation of Polymer Electrolytes Based on Poly(Ethylene Oxide) and Ionic Liquids. II. Dynamical Properties. *J. Chem. Phys.* **2007**, *127* (16), 164901.

(21) Kim, S. Y.; Park, M. J.; Balsara, N. P.; Jackson, A. Confinement Effects on Watery Domains in Hydrated Block Copolymer Electrolyte Membranes. *Macromolecules* **2010**, *43* (19), 8128–8135.

(22) Hazelbaker, E. D.; Guillet-Nicolas, R.; Thommes, M.; Kleitz, F.; Vasenkov, S. Influence of Confinement in Mesoporous Silica on Diffusion of a Mixture of Carbon Dioxide and an Imidazolium-Based Ionic Liquid by High Field Diffusion NMR. *Microporous Mesoporous Mater.* **2015**, *206*, 177–183.

(23) Nayeri, M.; Aronson, M. T.; Bernin, D.; Chmelka, B. F.; Martinelli, A. Surface Effects on the Structure and Mobility of the Ionic Liquid C6C1ImTFSI in Silica Gels. *Soft Matter* **2014**, *10* (30), 5618–5627.

(24) Han, K. S.; Wang, X.; Dai, S.; Hagaman, E. W. Distribution of 1-Butyl-3-Methylimidazolium Bistrifluoromethylsulfonimide in Mesoporous Silica As a Function of Pore Filling. *J. Phys. Chem. C* **2013**, *117* (30), 15754–15762.

(25) Shin, J. Y.; Yamada, S. A.; Fayer, M. D. Carbon Dioxide in a Supported Ionic Liquid Membrane: Structural and Rotational Dynamics Measured with 2D IR and Pump–Probe Experiments. *J. Am. Chem. Soc.* **2017**, *139* (32), 11222–11232.

(26) Labropoulos, A. I.; Romanos, G. E.; Kouvelos, E.; Falaras, P.; Likodimos, V.; Francisco, M.; Kroon, M. C.; Iliev, B.; Adamova, G.; Schubert, T. J. S. Alkyl-Methylimidazolium Tricyanomethanide Ionic Liquids under Extreme Confinement onto Nanoporous Ceramic Membranes. *J. Phys. Chem. C* **2013**, *117* (19), 10114–10127.

(27) Banu, L. A.; Wang, D.; Baltus, R. E. Effect of Ionic Liquid Confinement on Gas Separation Characteristics. *Energy & Fuels* **2013**, *27* (8), 4161–4166.

(28) Jang, S.; Kim, S. Y.; Jung, H. Y.; Park, M. J. Phosphonated Polymers with Fine-Tuned Ion Clustering Behavior: Toward Efficient Proton Conductors. *Macromolecules* **2018**, *51* (3), 1120–1128.

(29) Park, M. J. Confinement-Entitled Morphology and Ion Transport in Ion-Containing Polymers. *Mol. Syst. Des. Eng.* **2019**, *4* (2), 239–251.

(30) Bielejewski, M.; Puszkarska, A.; Tritt-Goc, J. Thermal Properties, Conductivity, and Spin-Lattice Relaxation of Gel Electrolyte Based on Low Molecular Weight Gelator and Solution of High Temperature Ionic Liquid. *Electrochim. Acta* **2015**, *165*, 122–129.

(31) Rachocki, A.; Andrzejewska, E.; Dembna, A.; Tritt-Goc, J. Translational Dynamics of Ionic Liquid Imidazolium Cations at Solid/Liquid Interface in Gel Polymer Electrolyte. *Eur. Polym. J.* **2015**, *71*, 210–220.

(32) Baltus, R. E.; Culbertson, B. H.; Dai, S.; Luo, H.; DePaoli, D. W. Low-Pressure Solubility of Carbon Dioxide in Room-Temperature Ionic Liquids Measured with a Quartz Crystal Microbalance. *J. Phys. Chem. B* **2004**, *108* (2), 721–727.

(33) Camper, D.; Scovazzo, P.; Koval, C.; Noble, R. Gas Solubilities in Room-Temperature Ionic Liquids. *Ind. Eng. Chem. Res.* **2004**, *43* (12), 3049–3054.

(34) Scovazzo, P.; Camper, D.; Kieft, J.; Poshusta, J.; Koval, C.; Noble, R. Regular Solution Theory and CO2 Gas Solubility in Room-Temperature Ionic Liquids. *Ind. Eng. Chem. Res.* **2004**, *43* (21), 6855–6860.

(35) Cadena, C.; Anthony, J. L.; Shah, J. K.; Morrow, T. I.; Brennecke, J. F.; Maginn, E. J. Why Is CO2 So Soluble in Imidazolium-Based Ionic Liquids? *J. Am. Chem. Soc.* **2004**, *126* (16), 5300–5308.

(36) Blanchard, L. A.; Gu, Z.; Brennecke, J. F. High-Pressure Phase Behavior of Ionic Liquid/CO2 Systems. *J. Phys. Chem. B* **2001**, *105* (12), 2437–2444.

(37) Lee, Y.-Y.; Edgehouse, K.; Klemm, A.; Mao, H.; Pentzer, E.; Gurkan, B. Capsules of Reactive Ionic Liquids for Selective Capture of Carbon Dioxide at Low Concentrations. *ACS Appl. Mater. Interfaces* **2020**, *12* (16), 19184–19193.

(38) Huang, Q.; Luo, Q.; Wang, Y.; Pentzer, E.; Gurkan, B. Hybrid Ionic Liquid Capsules for Rapid CO2 Capture. *Ind. Eng. Chem. Res.* **2019**, *58* (24), 10503–10509.

(39) Qavi, S.; Lindsay, A. P.; Firestone, M. A.; Foudazi, R. Ultrafiltration Membranes from Polymerization of Self-Assembled Pluronic Block Copolymer Mesophases. *J. Memb. Sci.* **2019**, *580*, 125–133.

(40) Qavi, S.; Bandegi, A.; Firestone, M.; Foudazi, R. Polymerization in Soft Nanoconfinements of Lamellar and Reverse Hexagonal Mesophases. *Soft Matter* **2019**, *15* (41), 8238–8250.

(41) Qavi, S.; Firestone, M. A.; Foudazi, R. Elasticity and Yielding of Mesophases of Block Copolymers in Water–Oil Mixtures. *Soft Matter* **2019**, *15* (28), 5626–5637.

(42) Qavi, S.; Foudazi, R. Rheological Characteristics of Mesophases of Block Copolymer Solutions. *Rheol. Acta* **2019**, *58* (8), 483–498.

(43) Saadat, Y.; Kim, K.; Foudazi, R. Initiator-Dependent Kinetics of Lyotropic Liquid Crystal-Templated Thermal Polymerization. *Polym. Chem.* **2021**.

(44) Jayaraman, A.; Zhang, D. Y.; Dewing, B. L.; Mahanthappa, M. K. Path-Dependent Preparation of Complex Micelle Packings of a Hydrated Diblock Oligomer. *ACS Cent. Sci.* **2019**, *5* (4), 619–628.

(45) Halperin, A.; Tirrell, M.; Lodge, T. P. Tethered Chains in Polymer Microstructures. In *Macromolecules: Synthesis, Order and Advanced Properties*; Springer Berlin Heidelberg: Berlin, Heidelberg, 1992; pp 31–71.

(46) Unsworth, L. D.; Tun, Z.; Sheardown, H.; Brash, J. L. Chemisorption of Thiolated Poly (Ethylene Oxide) to Gold: Surface Chain Densities Measured by Ellipsometry and Neutron Reflectometry. *J. Colloid Interface Sci.* **2005**, *281* (1), 112–121.

(47) Kim, M.; Schmitt, S. K.; Choi, J. W.; Krutty, J. D.; Gopalan, P. From Self-Assembled Monolayers to Coatings: Advances in the Synthesis and Nanobio Applications of Polymer Brushes. *Polymers (Basel).* **2015**, *7* (7), 1346–1378.

(48) Le Bideau, J.; Viau, L.; Vioux, A. Ionogels, Ionic Liquid Based Hybrid Materials. *Chem. Soc. Rev.* **2011**, *40* (2), 907–925.

(49) Bañuelos, J. L.; Feng, G.; Fulvio, P. F.; Li, S.; Rother, G.; Dai, S.; Cummings, P. T.; Wesolowski, D. J. Densification of Ionic Liquid Molecules within a Hierarchical Nanoporous Carbon Structure Revealed by Small-Angle Scattering and Molecular Dynamics Simulation. *Chem. Mater.* **2014**, *26* (2), 1144–1153.

(50) Bañuelos, J. L.; Feng, G.; Fulvio, P. F.; Li, S.; Rother, G.; Arend, N.; Faraone, A.; Dai, S.; Cummings, P. T.; Wesolowski, D. J. The Influence of a Hierarchical Porous Carbon Network on the Coherent Dynamics of a Nanoconfined Room Temperature Ionic Liquid: A Neutron Spin Echo and Atomistic Simulation Investigation. *Carbon N. Y.* **2014**, *78*, 415–427.

(51) Mogurampelly, S.; Ganesan, V. Structure and Mechanisms Underlying Ion

Transport in Ternary Polymer Electrolytes Containing Ionic Liquids. *J. Chem. Phys.* **2017**, *146* (7), 74902.

(52) Pradhan, D. K.; Choudhary, R. N. P.; Samantaray, B. K. Studies of Dielectric Relaxation and AC Conductivity Behavior of Plasticized Polymer Nanocomposite Electrolytes. *Int. J. Electrochem. Sci* **2008**, *3* (5), 597-608. www.electrochemsci.org/papers/vol3/305059.

(53) Bandegi, A.; Bañuelos, J. L.; Foudazi, R. Formation of Ion Gels by Polymerization of Block Copolymer/Ionic Liquid/Oil Mesophases. *Soft Matter* **2020**, *16* (26), 6102–6114.

(54) Sengwa, R. J.; Choudhary, S. Dielectric Relaxation Spectroscopy and X-Ray Diffraction Studies of Poly (Ethylene Oxide)–Lithium Perchlorate Electrolytes. *Indian J. Phys.* **2014**, *88* (5), 461–470.

(55) Choudhary, S.; Sengwa, R. J. Effects of Preparation Methods on Structure, Ionic Conductivity and Dielectric Relaxation of Solid Polymeric Electrolytes. *Mater. Chem. Phys.* **2013**, *142* (1), 172–181.

(56) Yao, M. L.; Watanabe, H.; Adachi, K.; Kotaka, T. Dielectric Relaxation Behavior of Styrene-Isoprene Diblock Copolymers: Bulk Systems. *Macromolecules* **1991**, *24* (10), 2955–2962.

(57) Wu, T.-Y.; Wang, H.-C.; Su, S.-G.; Gung, S.-T.; Lin, M.-W.; Lin, C.-B. Aggregation Influence of Polyethyleneglycol Organic Solvents with Ionic Liquids BMIBF4 and BMIPF6. *J. Chinese Chem. Soc.* **2010**, *57* (1), 44–55.

(58) Lee, H. N.; Newell, N.; Bai, Z. F.; Lodge, T. P. Unusual Lower Critical Solution Temperature Phase Behavior of Poly(Ethylene Oxide) in Ionic Liquids. *Macromolecules* **2012**, *45* (8), 3627–3633.

(59) Dyre, J. C. The Random Free-energy Barrier Model for Ac Conduction in Disordered Solids. *J. Appl. Phys.* **1988**, *64* (5), 2456–2468.

(60) Montroll, E. W.; Weiss, G. H. Random Walks on Lattices. II. *J. Math. Phys.* **1965**, *6* (2), 167–181.

(61) Macdonald, J. R. Utility of Continuum Diffusion Models for Analyzing Mobile-Ion Immittance Data: Electrode Polarization, Bulk, and Generation–Recombination Effects. *J. Phys. Condens. Matter* **2010**, *22* (49), 495101.

(62) Griffin, P. J.; Holt, A. P.; Wang, Y.; Novikov, V. N.; Sangoro, J. R.; Kremer, F.; Sokolov, A. P. Interplay Between Hydrophobic Aggregation and Charge Transport in the Ionic Liquid Methyltrioctylammonium Bis(Trifluoromethylsulfonyl)Imide. *J. Phys. Chem. B* **2014**, *118* (3), 783–790.

(63) Tokuda, H.; Hayamizu, K.; Ishii, K.; Susan, M. A. B. H.; Watanabe, M. Physicochemical Properties and Structures of Room Temperature Ionic Liquids. 1. Variation of Anionic Species. *J. Phys. Chem. B* **2004**, *108* (42), 16593–16600.

(64) Sangoro, J. R.; Serghei, A.; Naumov, S.; Galvosas, P.; Kärger, J.; Wespe, C.; Bordusa, F.; Kremer, F. Charge Transport and Mass Transport in Imidazolium-Based Ionic Liquids. *Phys. Rev. E* **2008**, *77* (5), 51202.

(65) Gainaru, C.; Stacy, E. W.; Bocharova, V.; Gobet, M.; Holt, A. P.; Saito, T.; Greenbaum, S.; Sokolov, A. P. Mechanism of Conductivity Relaxation in Liquid and Polymeric Electrolytes: Direct Link between Conductivity and Diffusivity. *J. Phys. Chem. B* **2016**, *120* (42), 11074–11083.

(66) Borodin, O.; Smith, G. D. Mechanism of Ion Transport in Amorphous Poly(Ethylene Oxide)/LiTFSI from Molecular Dynamics Simulations. *Macromolecules* **2006**, *39* (4), 1620–1629.

(67) Roy, A.; Dutta, B.; Bhattacharya, S. Correlation of the Average Hopping Length to the Ion Conductivity and Ion Diffusivity Obtained from the Space Charge Polarization in Solid Polymer Electrolytes. *RSC Adv.* **2016**, *6* (70), 65434–65442.

(68) Xiao, W.; Yang, Q.; Zhu, S. Comparing Ion Transport in Ionic Liquids and Polymerized Ionic Liquids. *Sci. Rep.* **2020**, *10* (1), 7825.

(69) Muldoon, M. J.; Aki, S. N. V. K.; Anderson, J. L.; Dixon, J. K.; Brennecke, J. F. Improving Carbon Dioxide Solubility in Ionic Liquids. *J. Phys. Chem. B* **2007**, *111* (30), 9001–9009.

(70) Klähn, M.; Seduraman, A. What Determines CO2 Solubility in Ionic Liquids? A Molecular Simulation Study. *J. Phys. Chem. B* **2015**, *119* (31), 10066–10078.

(71) Kazarian, S. G.; Briscoe, B. J.; Welton, T. Combining Ionic Liquids and Supercritical Fluids: In Situ ATR-IR Study of CO2 Dissolved in Two Ionic Liquids at High Pressures. *Chem. Commun.* **2000**, No. 20, 2047–2048.

(72) Ranjbaran, F.; Kamio, E.; Matsuyama, H. Ion Gel Membrane with Tunable Inorganic/Organic Composite Network for CO2 Separation. *Ind. Eng. Chem. Res.* **2017**, *56* (44), 12763–12772.

(73) Mahdavi, H. R.; Azizi, N.; Arzani, M.; Mohammadi, T. Improved CO2/CH4 Separation Using a Nanocomposite Ionic Liquid Gel Membrane. *J. Nat. Gas Sci. Eng.* **2017**, *46*, 275–288.

(74) Gu, Y.; Cussler, E. L.; Lodge, T. P. ABA-Triblock Copolymer Ion Gels for CO2 Separation Applications. *J. Membr. Sci.* **2012**, *423–424*, 20.